Supplementary information

Hepatic angiokine IFI16/IFI202 couples endothelial senescence and stellate cell activation to drive liver fibrosis

Ga Young Lim[1,*], Seung-Su Kim[1,*], Ji-Eun Kim[1], Hae-Min Kwon[1], Na-Lee Ka[2], Hyun Young Kim[3,4], Hyeon-Ji Kim[1], Sang-Heon Lee[1], Cheolhee Jeong[1], Yun-Hee Lee[1,5], Won Kim[6], Jihye You[7], You Mie Lee[7], Soo Young Park[8], and Mi-Ock Lee[1,5,9,**]

[1]College of Pharmacy and Natural Products Research Institute, Seoul National University, Seoul 08826, Republic of Korea.

[2]College of Pharmacy, Duksung Women's University, Seoul 01369, Republic of Korea.

[3]College of Pharmacy, Dankook University, Cheonan 31116, Republic of Korea.

[4]Center for Human Risk Assessment, Dankook University, Cheonan, Chungnam, Republic of Korea

[5]Research Institute of Pharmaceutical Sciences, Seoul National University, Seoul 08826, Republic of Korea.

[6]Department of Internal Medicine, Seoul National University College of Medicine, SMG-SNU Boramae Medical Center, Seoul 07061, Republic of Korea.

[7]Research Institute of Pharmaceutical Sciences, College of Pharmacy, Kyungpook National University, Daegu 41566, Republic of Korea.

[8]Department of Internal Medicine, School of Medicine, Kyungpook National University, Daegu 41944, Republic of Korea.

[9]Bio-MAX institute, Seoul National University, Seoul 08826, Republic of Korea.

*Equal contribution

**Corresponding author. Tel: +82 2 880 9331; E-mail: molee@snu.ac.kr

Address correspondence to: Mi-Ock Lee Ph. D., College of Pharmacy, Seoul National University, 1 Gwanak-ro, Gwanak-gu, Seoul 08826, Republic of Korea. E-mail: molee@snu.ac.kr

Supplementary Table 1. Reagents and resources used in this study

REAGENT or RESOURCE	SOURCE	IDENTIFIER
Antibodies		
anti-IFI202	Santa Cruz Biotechnology, Dallas, TX, USA	sc-166253
anti-IFI203	Prosci, Fort Collins, CO, USA	43-316
anti-IFI204	Novus Biologicals, Centennial, CO, USA	NBP2-27153
anti-p-STING	Cell Signaling Technology, Danvers, MA, USA	85735S
anti-STING	Cell Signaling Technology	13647S
anti-IFNβ	Invitinrogen, Thermo Fisher Scientific, Waltham, MA, USA	pa5-20390
anti-HSP60	Abcam	ab45134
anti-CD146	Abcam, Cambridge, UK	ab75769
anti-COL1A2	Santa Cruz Biotechnology	sc-8787
anti-PAI-1	BD Biosciences, San Jose, CA, USA	612024
anti-GSDMD	Invitrogen	PA50116815
anti-His	Santa Cruz Biotechnology	sc-8036
anti-α-SMA	Cell Signaling Technology	19245S
anti-MMP9	Santa Cruz Biotechnology	sc-10737
anti-MMP12	Proteintech, Rosemont, IL, USA	22989-1-AP
anti-P21	Santa Cruz Biotechnology	sc-6246
anti-TGFβ	Santa Cruz Biotechnology	sc-374658
anti-p-ERK	Santa Cruz Biotechnology	sc-7383
anti-ERK	Santa Cruz Biotechnology	sc-94
anti-p-p65	Cell Signaling Technology	3033S
anti-p65	Cell Signaling Technology	19781S
anti-p-SMAD3	Cell Signaling Technology	9520S
anti-SMAD2/3	Cell Signaling Technology	3102S
anti-LAMIN B1	Abcam	ab16048
anti-cKIT	R&D Systems, Minneapolis, MN, USA	AF1356
anti-LYVE1	Abcam	ab281587
anti-p-eNOS	Cell Signaling Technology	9570
anti-eNOS	Cell Signaling Technology	32027
Virus strains		
pAAV-MCS	Cell Biolabs, San Diego, CA, USA	VPK-410

Chemicals		
Corn oil	Sigma-Aldrich	8001-30-7
CCl_4	Sigma-Aldrich	56-23-5
DDC	Sigma-Aldrich	137030
CD146 Microbeads	Miltenyi Biotec, Bergisch Gladbach, Germany	130-092-007
IFN-β	PBL Assay Science, Piscataway, NJ, USA	12410-1
Hydrogen peroxide	Sigma-Aldrich	H1009
mIL-6	PeproTech, Cranbury, NJ, USA	216-16
mTGF-β	R&D Systems	7666-MB-005
Chenodeoxycholic acid	Sigma-Aldrich	C9377
Necrosulfonamide	Sigma-Aldrich	480073
IgG isotype control	GenScript, Piscataway, NJ, USA	A01730
Lipofectamine 2000	Invitrogen	11668019
C-176	MedChemExpress	HY-112906
C29	InvivoGen.	inh-c29
OxPAPC	InvivoGen.	tlrl-oxp1
Lipofectamine 3000	Invitrogen	L3000001
Dexamethasone	Sigma-Aldrich, St. Louis, MO, USA	D4902
Easy-Blue	iNtRON Biotechnology, Seongnam, South Korea	17061
PMSF	Sigma-Aldrich	P7626
SYBR Green Master mix	Applied Biosystems, Thermo Fisher Scientific, Waltham, MA, USA	A25742
A-coated magnetic beads	GenScript, Piscataway, NJ, USA	
Insulin–transferrin–selenium	Thermo Fisher Scientific	41400045
Critical commercial assays		
Human IFI16 ELISA kit	LSBio	LS-F27011
Mouse Interferon-activable protein 202 (IFI202) ELISA Kit	Abbexa, Cambridge, UK	abx528062
Senescence Cells histochemical Staining kit	Sigma-Aldrich	CS0030
LDH cytotoxicity assay kit	Sigma-Aldrich	MAK529
Mouse IL-6 ELISA Kit	R&D Systems	M6000B
Mouse TNF-alpha ELISA Kit	R&D Systems	MTA00B
Mouse IL-1 beta/IL-1F2 ELISA Kit	R&D Systems	MLB00C
Corning® spheroid microplates	Sigma-Aldrich	4515

Isostrip Mouse Monoclonal Isotyping Kit	Roche, Basel, Switzerland	
SBA Clonotyping System-HRP kit	SouthernBiotech, Birmingham, AL, USA	
Nitric Oxide Assay Kit (Colorimetric)	Abcam	ab65328
Software and algorithms		
R	R Core Team, Vienna, Austria	4.2.2.
Alphafold2	DeepMind, London, UK; EMBL-EBI, Hinxton, Cambridgeshire, UK	
Prism	GraphPad Prism, GraphPad Software, San Diego, CA, USA	Version 9
Phenochart™	PerkinElmer, Waltham, MA, USA	Version 2
LAS-X	Leica Microsystems, Wetzlar, Germany	Version 1
Image J	National Institutes of Health	https://imagej.nih.gov/ij/
GraphPad Prism software	GraphPad Software, San Diego, CA, USA	
Others		
CDAA-HFD	Research Diets, Inc., New Brunswick, NJ, USA	A06071302
FUJI DRI-CHEM 3500s	Fujifilm, Tokyo, Japan	

Supplementary Table 2. Oligonucleotide sequences used in the present investigation.

Purpose	Gene	Accession number		Nucleotide sequence
shRNA IFI202	*Ifi202*	NM_008327.2	Sense Antisense	5'- GAGAAAAGGAAATGGGAAACC-3' 5'- TCAATGCCACCACTTGTTTG-3'
siRNA	*GFP*		Sense Antisense	5'- GUUCAGCCUGUCCGGCGAG-3' 5'- CUCGCCGGACAGGCUGAAC-3
	TLR2-1	NM_011905.3	Sense Antisense	5- AACGAAAAGCAGAGAAGUG-3 5- CACUUCUCUGCUUUUCGUU-3´
	TLR2-2	NM_011905.3	Sense Antisense	5- AAUGAUUCUGGCUCAAAAC-3´ 5- GUUUUGAGCCAGAAUCAUU-3´
qRT-PCR	*Ifi202*	NM_008327.2	Sense Antisense	5'- GGCAATGTCCAACCGTAACT-3' 5'- TAGGTCCAGGAGAGGCTTGA-3'
	Lyve1	NM_053247.4	Sense Antisense	5'- CAGCACACTAGCCTGGTGTTA-3' 5'- CGCCCATGATTCTGCATGTAGA-3'
	Pecam1	NM_001032378.3	Sense Antisense	5'- ACCGGGTGCTGTTCTATAAGG-3' 5'- TCACCTCGTACTCAATCGTGG-3'
	Edn1	NM_010104.4	Sense Antisense	5'- CACCGTCCTCTTCGTTTTGC-3' 5'- GGCTCTGCACTCCATTCTCA-3'
	Lamb1	NM_008482.3	Sense Antisense	5'-GAAAGGAAGACCCGAAGAAAA-3' 5'-CCATAGGGCTAGGACACCAAA-3'
	Stab2	NM_138673.3	Sense Antisense	5'- AACTGGCAGTGATGTCGGAG-3' 5'- GGAGTGGAGAAACAGCTCCC-3'
	Cd209b	NM_026972.5	Sense Antisense	5'-TGGGCTCCTGCTGATCATT-3' 5'-TTCCCTTGGGAGATGGGGAT-3'
	Ehd3	NM_020578.3	Sense Antisense	5'-CGCCGTGCTTGAAAGTATCAG-3' 5'-ATAATTCGGTCCACCCGCTC-3'
	Plvap	NM_032398.2	Sense Antisense	5'-CCTGCGCTATTTCTTCCTCTT-3' 5'- CAGTTGCTGCATGACTGTTTC-3'
	Stab1	NM_138672.2	Sense Antisense	5'- TCACTGTCCCCACACTACTTT -3' 5'- TGTCGCAACGTTTAGACCGTA -3'
	Nos3	NM_008713.4	Sense Antisense	5'- TGAGTTCAGAGATTGGCATGAG-3' 5'- CTTGATGGAAGACAGGAGTTAGG-3'
	Cdkn2a	NM_001040654.1	Sense Antisense	5'-CGAACTCGAGGAGAGCCATC-3' 5'-TACGTGAACGTTGCCCATCA-3'
	Cdkn1a	NM_007669.5	Sense Antisense	5'-AAGTGTGCCGTTGTCTCTTC -3' 5'-AGTCAAAGTTCCACCGTTCTC-3'

Supplementary Table 3. Top 21 transcripts differentially expressed in fibrotic human livers relative to healthy livers across three datasets

Gene symbol	Full Name	Accession number	Fold Change
			GSE206364
COL4A2	Collagen Type IV Alpha 2 Chain	NM_001846.4	2.76
TPM1	Tropomyosin 1	NM_001018005.2	1.78
GSN	Gelsolin	NM_198252.3	2.16
COL4A1	Collagen Type IV Alpha 1 Chain	NM_001845.5	2.85
PACS1	Phosphofurin Acidic Cluster Sorting Protein 1	NM_018026.4	1.30
IFI16	Interferon Gamma Inducible Protein 16	NM_005531.5	2.23
UGCG	UDP-Glucose Ceramide Glucosyltransferase	NM_003358.3	1.70
SEL1L3	SEL1L Family Member 3	NM_015187.5	2.12
HKDC1	Hexokinase Domain Containing 1	NM_025130.4	3.98
CBLB	Casitas B-Lineage Lymphoma Proto-Oncogene B	NM_170662.5	1.86
GLS	Glutaminase	NM_014905.5	2.04
RAB8B	RAB8B, Member RAS Oncogene Family	NM_016530.3	1.79
DCDC2	Doublecortin Domain Containing 2	NM_016356.5	3.75
BACE2	Beta-Secretase 2	NM_012105.5	2.37
SLCO3A1	Solute Carrier Organic Anion Transporter Family Member 3A1	NM_013272.4	1.77
BICC1	BicC Family RNA Binding Protein 1	NM_001080512.3	3.11
GPRIN3	G Protein Regulated Inducer of Neurite Outgrowth 3	NM_198281.3	3.61
DTNA	Dystrobrevin Alpha	NM_001386795.1	3.82
ARHGEF3	Rho Guanine Nucleotide Exchange Factor 3	NM_019555.3	2.61
SLC22A15	Solute Carrier Family 22 Member 15	NM_018420.3	3.83

Supplementary Figures

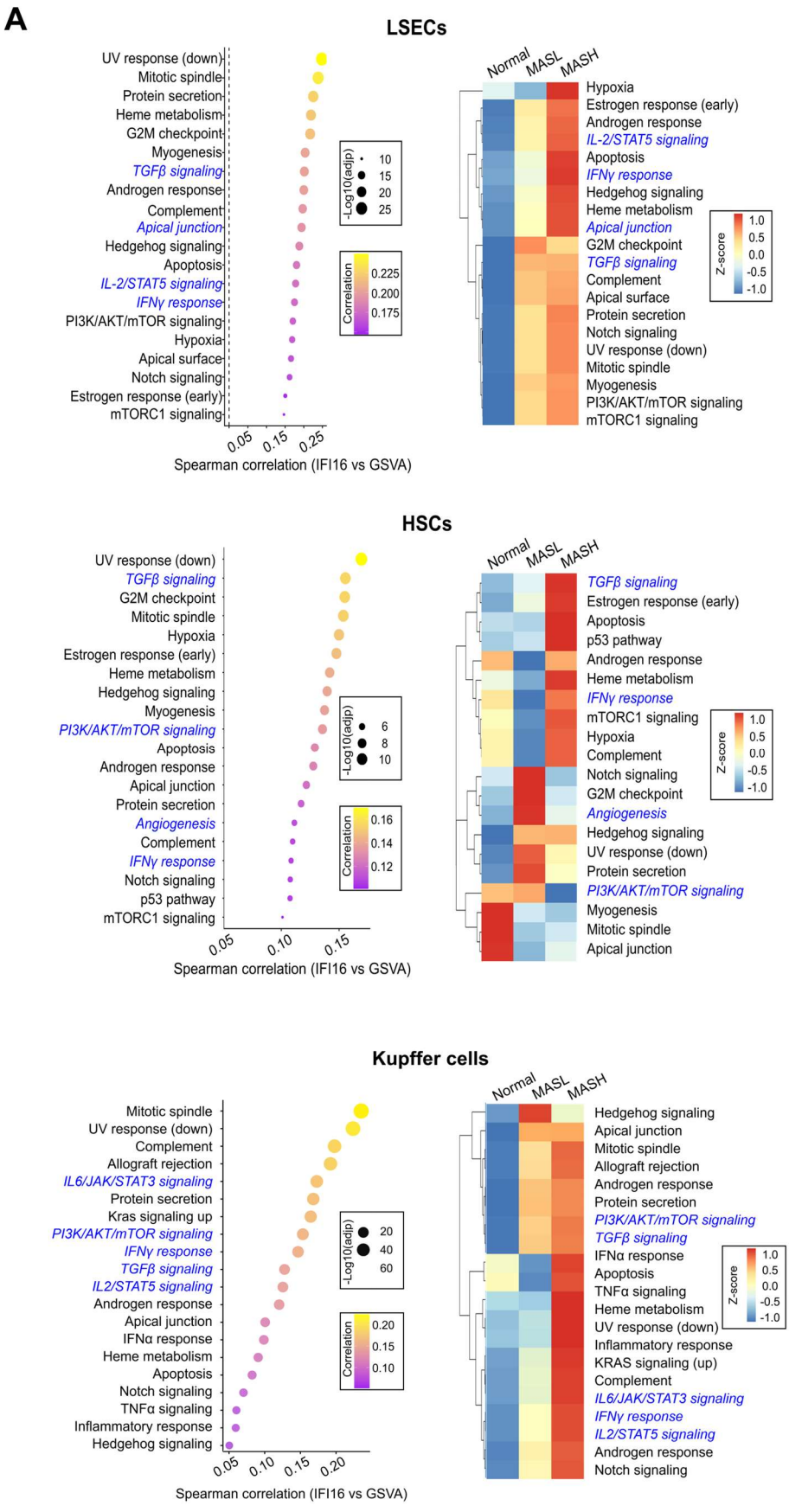

B

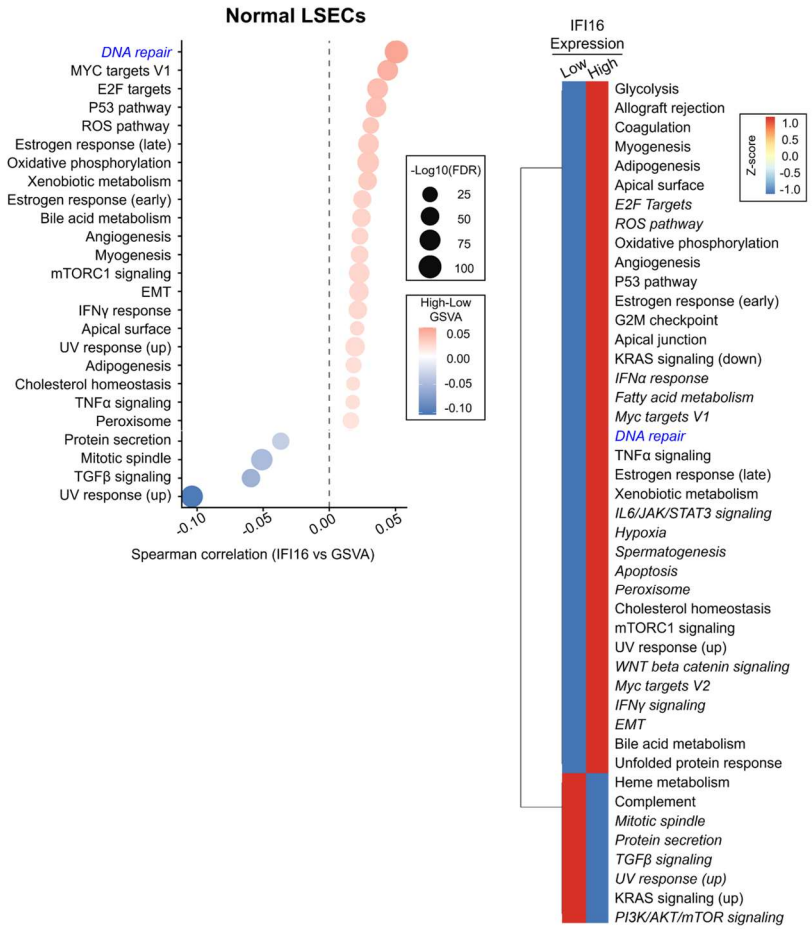

C

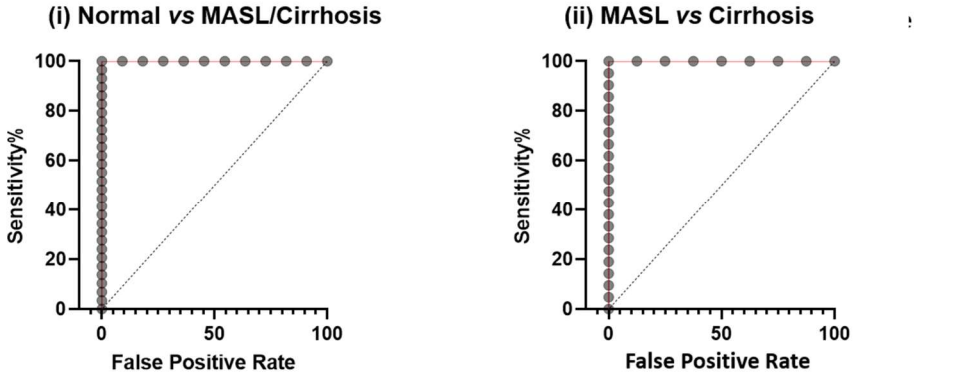

Area	1.000
Std. Error	0.000
95% confidence interval	1.000 to 1.000
P value	<0.0001

Area	1.000
Std. Error	0.000
95% confidence interval	1.000 to 1.000
P value	<0.0001

Supplementary Figure 1: IFI16-associated transcriptional programs in LSECs, HSCs and Kupffer cells across disease progression.

(A) IFI16-associated transcriptional programs in LSECs, HSCs and Kupffer cells across disease progression. Dot plots and heatmaps showing IFI16-associated gene sets identified by GSVA and correlation analysis in LSEC (top), HSC (middle) and Kupffer cells (bottom). Dot plots display the Hallmark gene sets positively correlated with IFI16 expression, ranked by Spearman correlation coefficient. Dot size represents statistical significance (−log10 adjusted p-value), and color indicates the strength of correlation. Corresponding heatmaps illustrate the average GSVA scores of these gene sets across disease conditions (Normal, MASL, and MASH), scaled by row. Rows represent gene sets, and columns represent disease conditions. **(B)** Physiological pathways associated with IFI16 expression in normal LSECs. A total of 7,395 endothelial cells were identified, of which 1,638 cells exhibited detectable IFI16 expression (IFI16 > 0). IFI16-positive endothelial cells were stratified into IFI16-low (*n = 410*) and IFI16-high (*n = 411*) groups using the lower and upper quartiles of log-normalized IFI16 expression (Q1 = 1.724, Q3 = 2.443), while cells with intermediate IFI16 expression (*n = 817*) were excluded from the comparison. Differential pathway activity between IFI16-high and IFI16-low LSECs was evaluated using the Wilcoxon rank-sum test followed by Benjamini–Hochberg multiple-testing correction. Forty-five Hallmark pathways were significantly altered at an FDR < 0.05. The heatmap displays row-scaled mean GSVA scores for representative pathways, whereas the accompanying dot plot shows the top 21 pathways ranked by statistical significance and effect size. Dot color represents the mean GSVA score difference between IFI16-high and IFI16-low LSECs (High − Low), and dot size represents the statistical significance (−log10 adjusted P value). **(C)** Receiver operating characteristic (ROC) curve analysis of circulating IFI16 levels in patients with MASLD. ROC curve analysis was performed to evaluate the diagnostic performance of serum IFI16 levels. (i) ROC curve distinguishing healthy controls from patients with liver disease (MASL and cirrhosis). (ii) ROC curve distinguishing patients with MASL from those with cirrhosis. The area under the ROC curve (AUC), 95% confidence intervals, and corresponding *P* values are indicated in each panel.

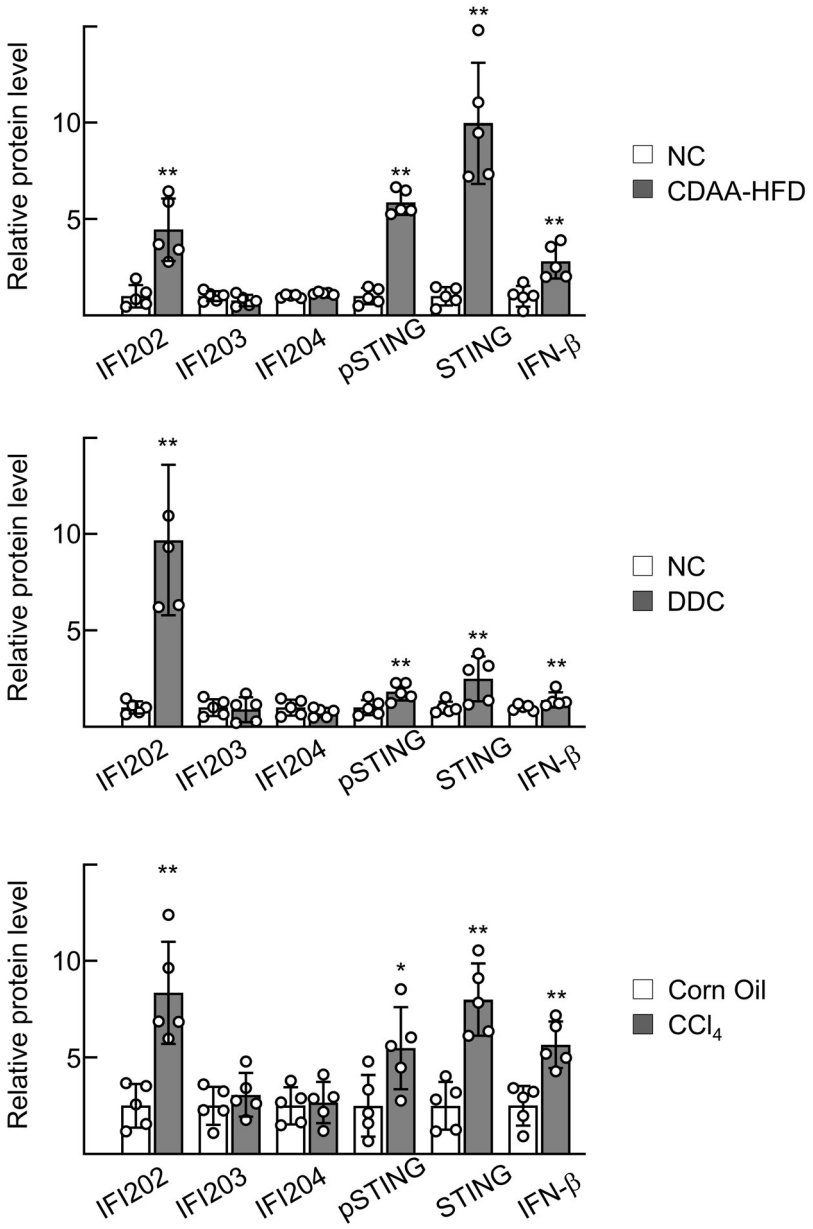

Supplementary Figure 2: Hepatic IFI202 expression is induced after fibrotic liver injury in mice (related to Figure 2).

Band intensities of western blot images shown in Figure 2A, 2B, and 2C were quantified using ImageJ software (National Institutes of Health). Data are presented as mean ± SD, $n = 5$ per group. Statistical significance was assessed using the two-tailed Mann–Whitney U test. $^{**}P < 0.01$ *vs* normal chow (NC) or corn oil, $^{*}P < 0.05$ *vs* NC or corn oil.

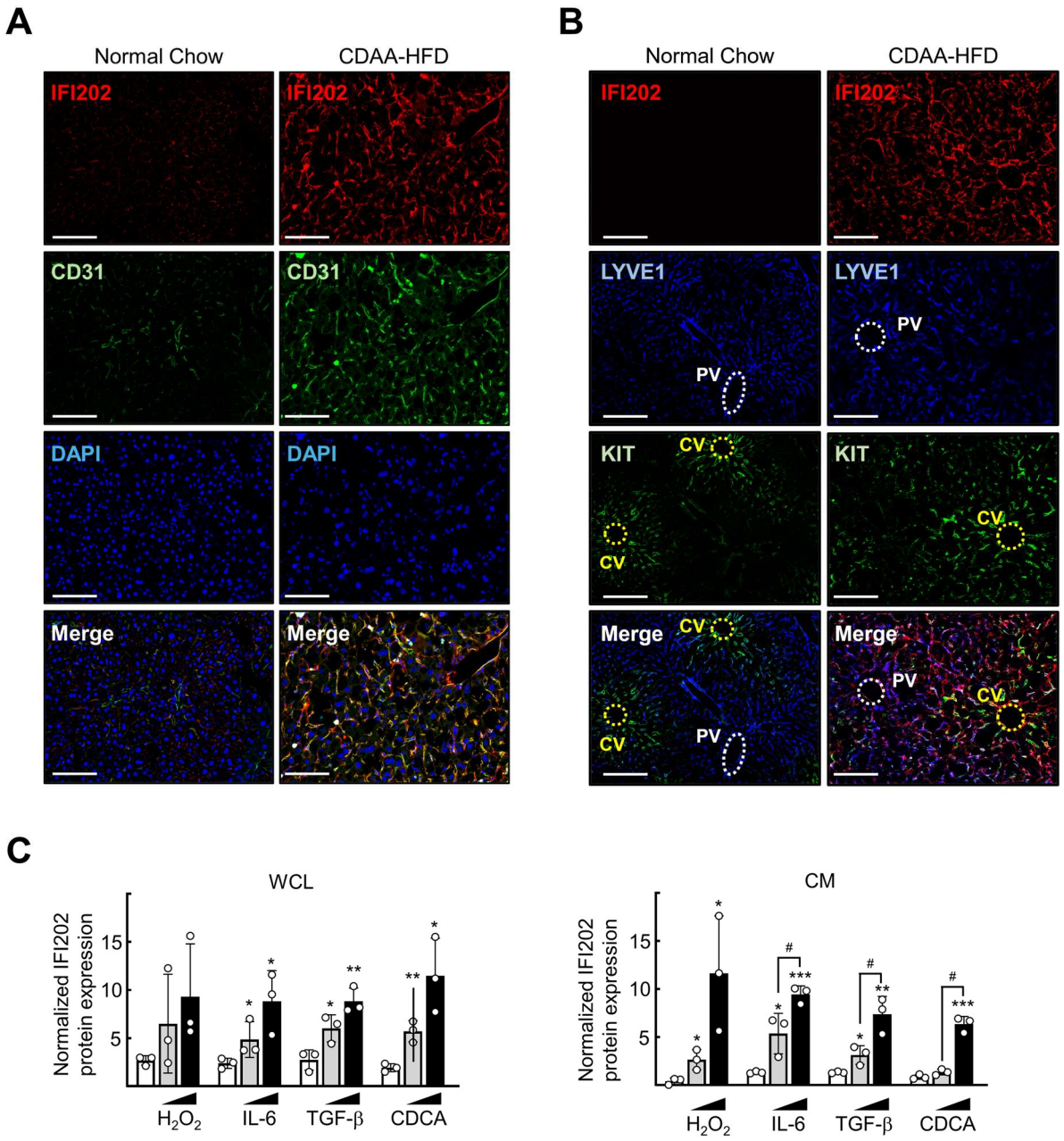

Supplementary Figure 3: Expression and secretion levels of IFI202 were elevated in primary LSECs upon stimulation with fibrogenic stimuli (related to Figure 3).

(**A, B**) Representative immunofluorescence images of liver sections from mice fed a CDAA-HFD. IFI202 (red), CD31 (green), and merged images (**A**). IFI202 (red), LYVE1 (blue), KIT (green), and merged images (**B**). Scale bar, 100 μm. (**C**) Band intensities of western blot images shown in Figure 3E was quantified using ImageJ software. Data are presented as mean ± SD (*n = 3*). Statistical significance was determined by unpaired *t*-test. $^{***}P < 0.001$ *vs* vehicle; $^{**}P < 0.01$ *vs* vehicle; $^{*}P < 0.05$ *vs* vehicle; $^{\#}P < 0.05$ *vs* the corresponding intermediate-dose group.

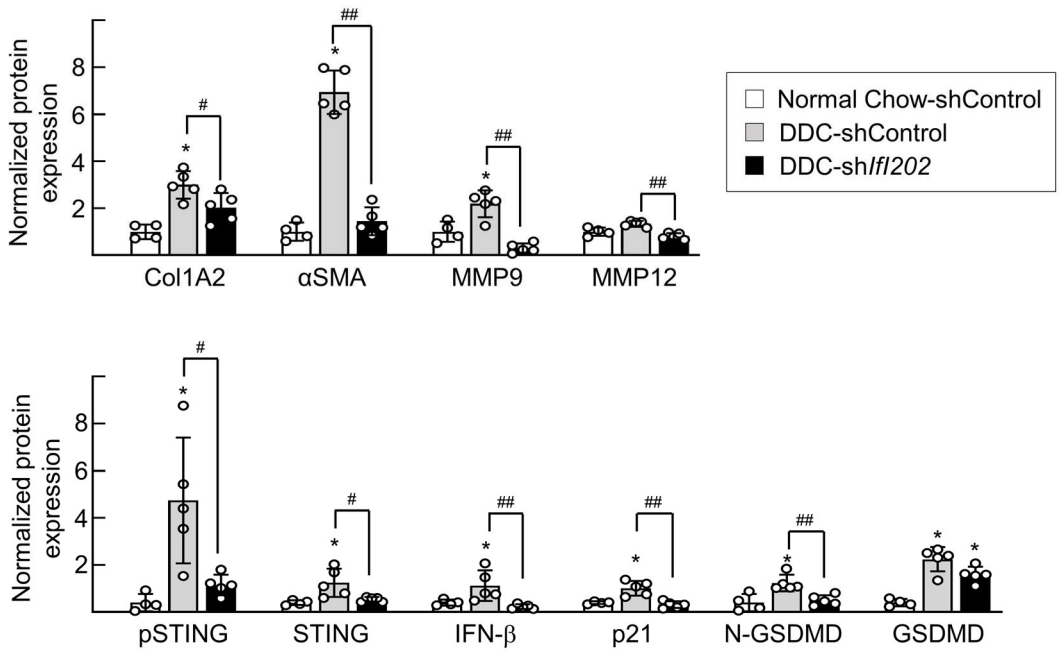

Supplementary Figure 4: Fibrotic liver injury induces IFI202 expression in the mouse liver (related to Figure 5)

Band intensities of western blot images shown in Figures 5B and 5C were quantified using ImageJ software. Data are presented as mean ± SD (*n = 4, 5, and 5* per group). Statistical significance was performed using the two-tailed Mann–Whitney *U* test. $^{*}P < 0.05$ *vs* NC–shControl; $^{\#\#}P < 0.01$ *vs* DDC–shControl; $^{\#}P < 0.05$ *vs* DDC–shControl.

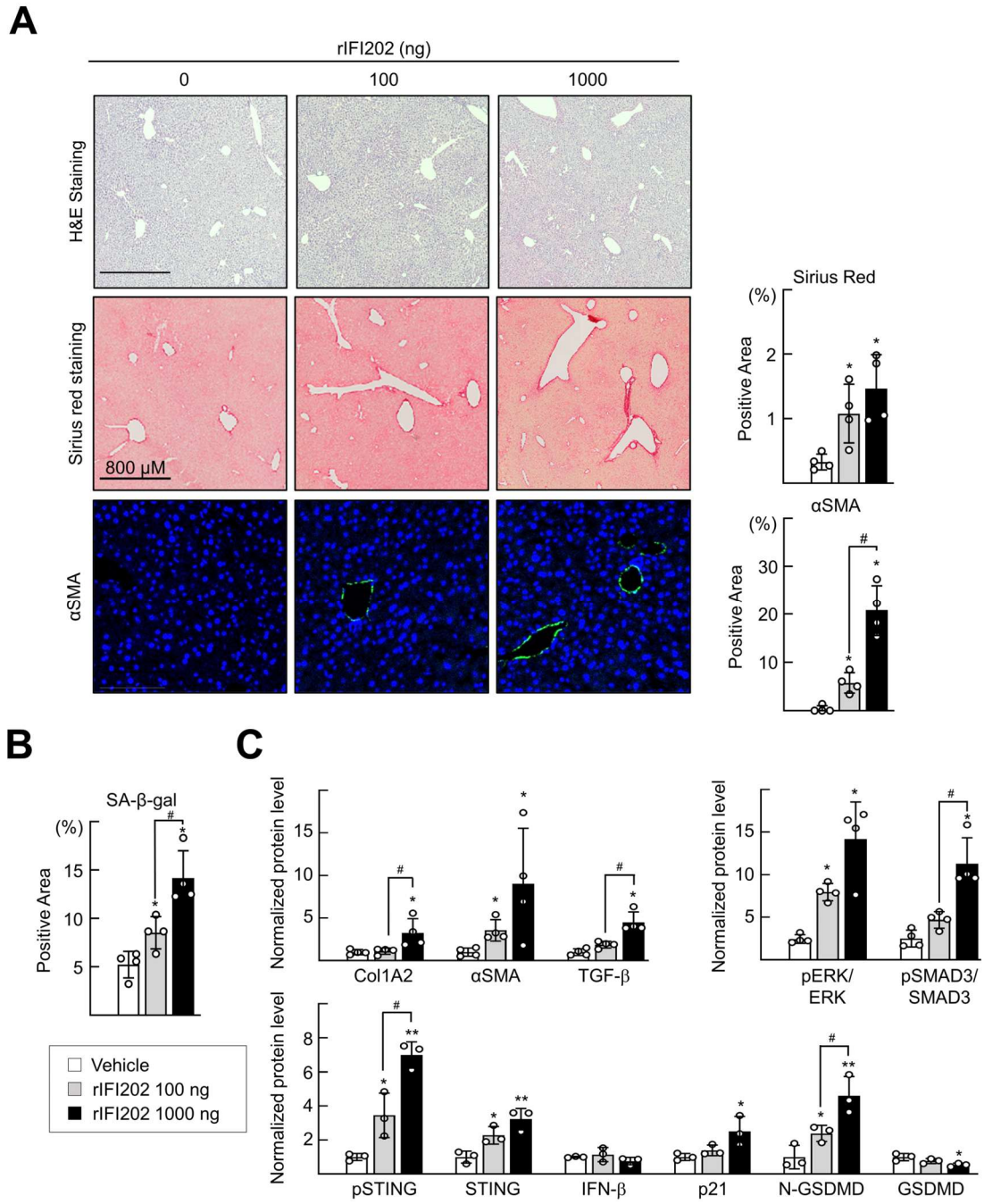

Supplementary Figure 5: Injection of IFI202 induces fibrotic changes in the liver (related to Figure 6).

(**A**) Representative images of liver sections stained with Sirius Red (top), immunofluorescence for αSMA (middle), H&E (bottom), scale bar, 800 µm (left). Staining intensity was quantified from four liver samples per group using ImageJ software (right). Data are presented as mean ± SD (*n = 4* per group). Statistical analyses were performed using the two-tailed Mann–Whitney *U* test. $^{*}P < 0.05$ *vs* Vehicle; $^{\#}P < 0.01$ *vs* rIFI202 100 ng. **(B)** Quantification of senescence associated-β-galactosidase (SA-β-gal)–positive cells corresponding to Figure 6D. Data are presented as mean ± SD (*n = 4* per group). Statistical analyses were performed using the two-tailed Mann–Whitney *U* test. $^{*}P < 0.05$ *vs* Vehicle;

$^{\#}P < 0.05$ *vs* rIFI202 100 ng. **(C)** Band intensities of western blot images shown in Figures 6C and 6D were quantified using ImageJ software. Data are presented as mean ± SD (*n = 4* per group). Statistical analysis was performed using the two-tailed Mann–Whitney *U* test. $^{**}P < 0.01$ *vs* Vehicle, $^{*}P < 0.05$ *vs* Vehicle; $^{\#}P < 0.05$ *vs* rIFI202 100 ng.

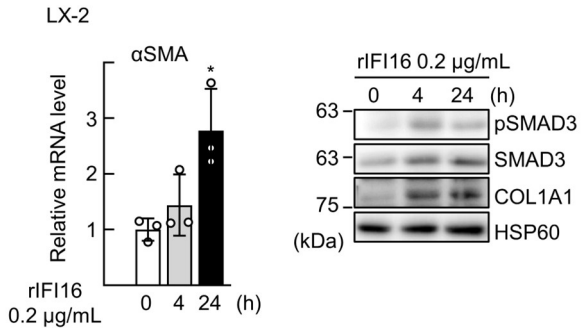

Supplementary Figure 6: IFI16 upregulated αSMA, COL1A1 and TLR2 downstream signaling in LX-2 human HSCs.

LX-2 cells (2×10^5 cells/well) were treated with recombinant human IFI16 (rIFI16; 0.2 μg/mL; OriGene) and harvested at 0, 4, and 24 h. The mRNA expression level of αSMA was analyzed by qRT-PCR (left). Data are presented as mean ± SD ($n = 3$). Statistical significance was determined using an unpaired *t*-test. $^{*}P < 0.05$ *vs* 0 h. Protein expression levels of pSMAD3, total SMAD3, and COL1A1 were assessed by western blotting (right). HSP60 was used as a loading control.

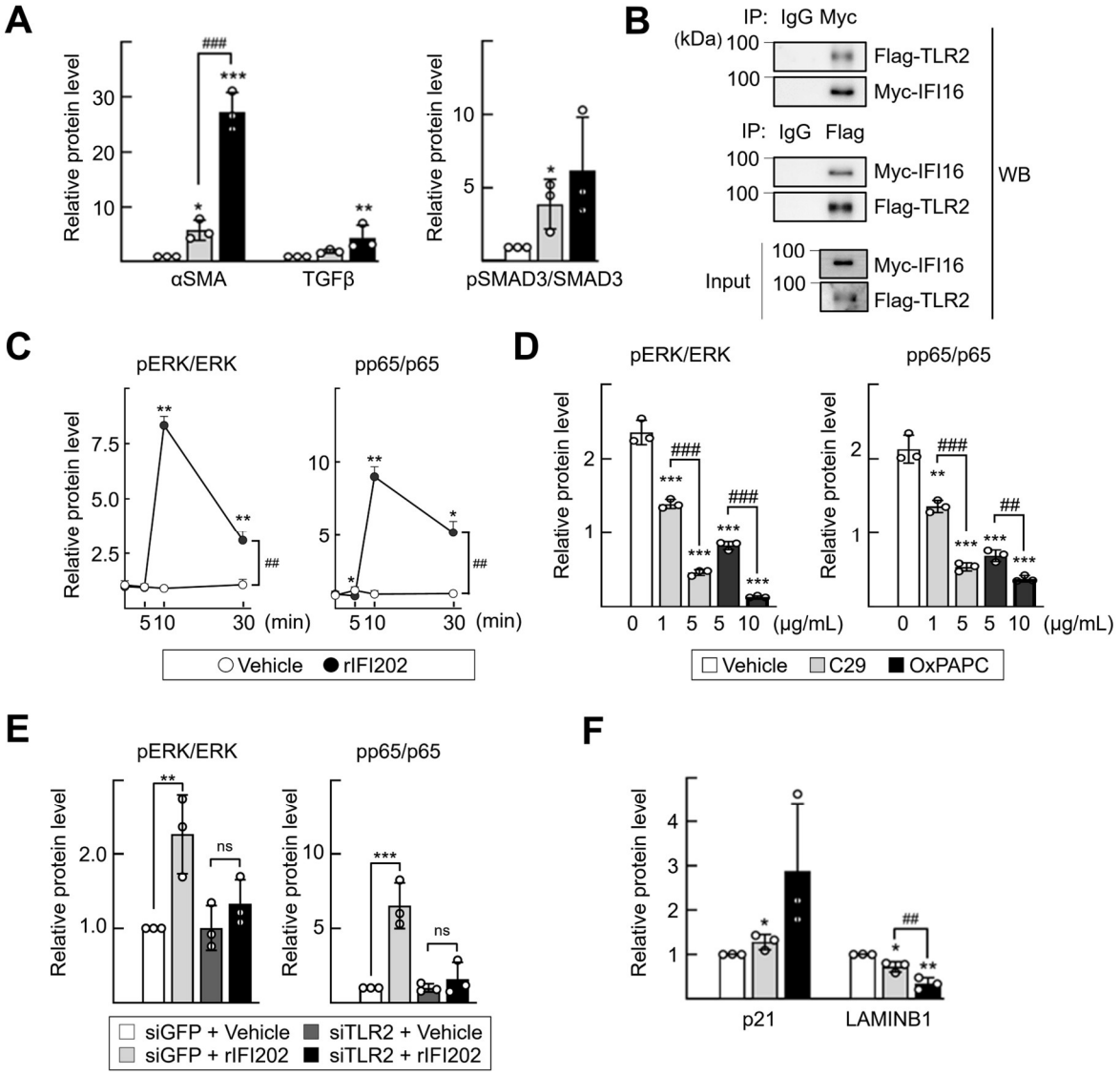

Supplementary Figure 7: rIFI202 induces TLR2-mediated activation of HSCs and senescence of LSECs (related to Figure 7).

(**A**) Band intensities of western blot images shown in Figure 7A were quantified using ImageJ software. Data are presented as mean ± SD (*n = 3*). Statistical significance was determined by unpaired *t*-test. $^{***}P < 0.001$ *vs* 0 h, $^{**}P < 0.01$ *vs* 0 h, $^{*}P < 0.05$ *vs* 0 h; $^{\#\#\#}P < 0.001$ *vs* 0 h. (**B**) Immunoprecipitation was performed using whole cell lysates from LX-2 cells overexpressing Myc-IFI16 and Flag-TLR2 using anti-Flag or anti-Myc antibodies, and the precipitated proteins were analyzed by western blot. **(C)** Band intensities of western blot images shown in Figure 7B were quantified using ImageJ software. Data are presented as mean ± SD (*n = 3* per group). Statistical significance was determined by two-way ANOVA with Bonferroni post hoc tests. $^{**}P < 0.01$, $^{*}P < 0.05$ *vs* Vehicle of each time point; $^{\#\#}P < 0.01$ *vs* Vehicle. (**D**) Band intensities of western blot images shown in Figure 7C (left) were quantified using ImageJ software. Data are presented as mean ± SD (*n = 3* per group). Statistical significance was determined by unpaired *t*-test. $^{***}P < 0.001$ *vs* Vehicle, $^{**}P < 0.01$ *vs* Vehicle; $^{\#\#\#}P < 0.001$ *vs* C29 1

μg/mL or OxPAPC 5 μg/mL, $^{\#\#}P < 0.01$ *vs* C29 1 μg/mL or OxPAPC 5 μg/mL. **(E)** Band intensities of western blot images shown in Figure 7C (right) were quantified using ImageJ software. The level of TLR2 proteins were suppressed by 79.1 ± 1.9% (mean ± SD, $n = 3$) in this siRNA approach. Data are presented as mean ± SD ($n = 3$). Statistical significance was determined by unpaired *t*-test. $^{**}P < 0.01$ and $^{***}P < 0.001$. ns, not significant. **(F)** Band intensities of western blot images shown in Figure 7D were quantified using ImageJ software. Data are presented as mean ± SD ($n = 3$). Statistical significance was determined by unpaired *t*-test. $^{**}P < 0.01$ *vs* 0 μg/mL, $^{*}P < 0.05$ *vs* 0 μg/mL; $^{\#\#\#}P < 0.001$ *vs* 0.2 μg/mL, $^{\#\#}P < 0.01$ *vs* 0.2 μg/mL.

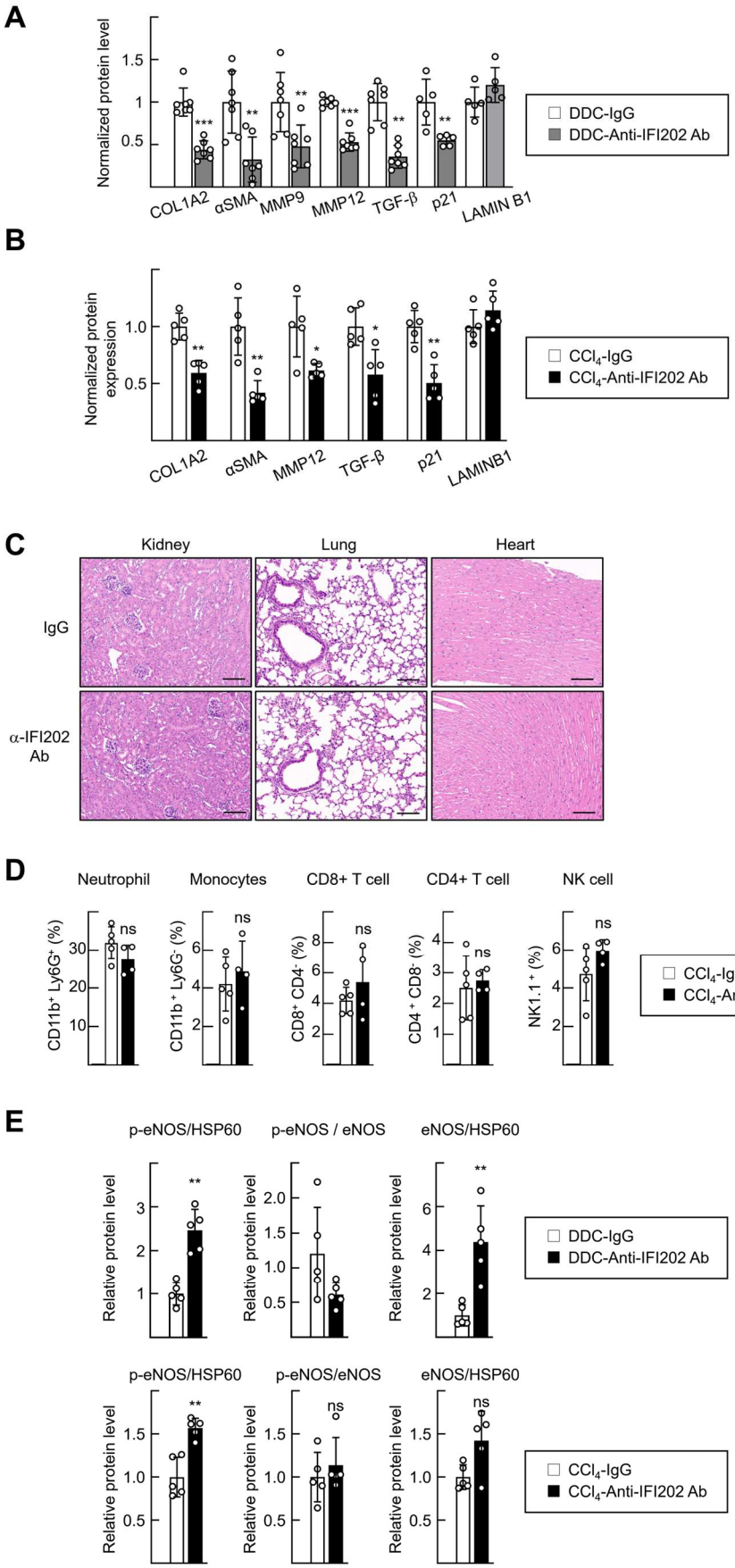
A
Normalized protein level
1.5
1
0.5
COL1A2
αSMA
MMP9
MMP12
TGF-β
p21
LAMIN B1
DDC-IgG
DDC-Anti-IFI202 Ab
B
Normalized protein expression
1.0
0.5
COL1A2
αSMA
MMP12
TGF-β
p21
LAMINB1
CCl4-IgG
CCl4-Anti-IFI202 Ab
C
Kidney
Lung
Heart
IgG
α-IFI202 Ab
D
Neutrophil
Monocytes
CD8+ T cell
CD4+ T cell
NK cell
CD11b+ Ly6G+ (%)
CD11b+ Ly6G- (%)
CD8+ CD4- (%)
CD4+ CD8- (%)
NK1.1+ (%)
ns
CCl4-IgG
CCl4-Anti-IFI202 Ab
E
p-eNOS/HSP60
p-eNOS / eNOS
eNOS/HSP60
Relative protein level
DDC-IgG
DDC-Anti-IFI202 Ab
p-eNOS/HSP60
p-eNOS/eNOS
eNOS/HSP60
Relative protein level
CCl4-IgG
CCl4-Anti-IFI202 Ab

Supplementary Figure 8: IFI202 neutralization attenuates fibrosis-related gene expression without apparent systemic or immunological effects.

(**A**) Band intensities of western blot images shown in Figure 8D were quantified using ImageJ software. Data are presented as mean ± SD (*n = 7* per group). Statistical significance was performed using two-tailed Mann–Whitney *U* test. $^{***}P < 0.001$ *vs* DDC–IgG, $^{**}P < 0.01$ *vs* DDC–IgG. **(B)** Band intensities of western blot images shown in Figure 8G were quantified using ImageJ software. Data are presented as mean ± SD (*n = 5* per group). Statistical analysis was performed using the Mann–Whitney *U* test. $^{*}P < 0.05$, $^{**}P < 0.01$ *vs* CCl_4–IgG. **(C)** Representative H&E-stained sections of the heart, lung, and kidney from CCl_4-treated mice treated with IgG or anti-IFI202 neutralizing antibody. Scale bars, 100 μm. **(D)** Flow-cytometric analysis of peripheral blood leukocytes from mice treated with CCl_4 together with control IgG or a neutralizing anti-IFI202 antibody for 4 weeks. The frequencies of neutrophils ($CD11b^+Ly6G^+$), monocytes ($CD11b^+Ly6G^-$), $CD8^+$ T cells ($CD8^+CD4^-$), $CD4^+$ T cells ($CD4^+CD8^-$), and NK cells ($NK1.1^+$) are shown as percentages of $CD45^+$ cells. Data are presented as individual values with mean ± SEM. ns, not significant. **(E)** Band intensities of western blot images shown in Figure 8H were quantified using ImageJ software. Data are presented as mean ± SD (*n = 5* per group). Statistical analysis was performed using the Mann–Whitney *U* test. $^{*}P < 0.05$, $^{**}P < 0.01$ *vs* DDC-IgG or CCl_4–IgG.

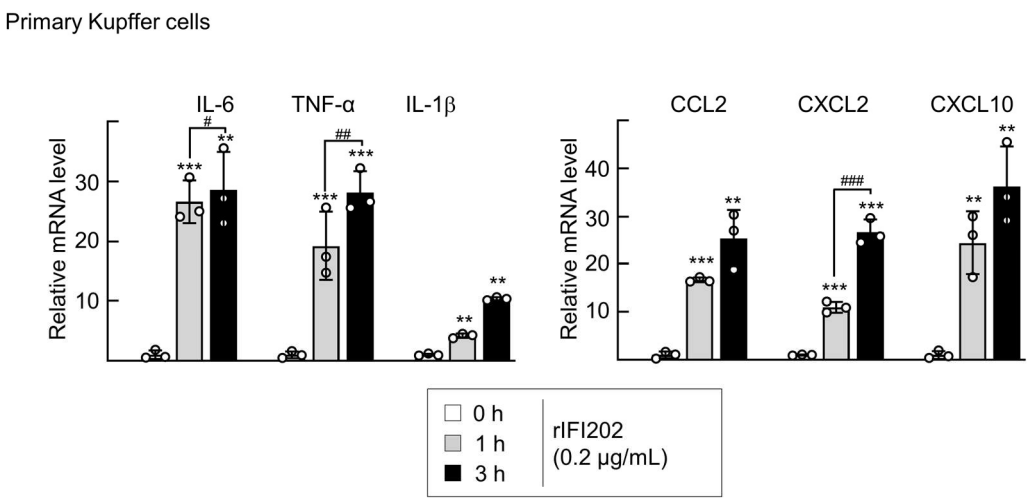

Supplementary Figure 9: IFI202 induces proinflammatory cytokines and chemokines in KCs. Primary KCs (1×10^6 cells/well) were treated with recombinant mouse IFI202 (rIFI202; 0.2 μg/mL) and harvested at 0, 1, and 3 h. The mRNA expression levels of proinflammatory cytokines and chemokines were measured by qRT-PCR. Data are presented as mean ± SD ($n = 3$). Statistical significance was assessed using an unpaired *t*-test. $^{***}P < 0.001$ *vs* 0 h, $^{**}P < 0.01$ *vs* 0 h; $^{###}P < 0.001$ *vs* 1 h, $^{##}P < 0.01$ *vs* 1 h, $^{#}P < 0.05$ *vs* 1 h.